IOPscience iopscience.iop.org

Home Search Collections Journals About Contact us My IOPscience

Casimir rack and pinion

This article has been downloaded from IOPscience. Please scroll down to see the full text article.

2007 J. Phys.: Conf. Ser. 89 012017

(http://iopscience.iop.org/1742-6596/89/1/012017)

View the table of contents for this issue, or go to the journal homepage for more

Download details:
IP Address: 163.1.203.196
The article was downloaded on 23/08/2013 at 08:53

Please note that terms and conditions apply.

Journal of Physics: Conference Series **89** (2007) 012017 doi:10.1088/1742-6596/89/1/012017

Casimir Rack and Pinion

Arash Ashourvan
Institute for Advanced Studies in Basic Sciences, Zanjan, 45195-1159, Iran

MirFaez Miri
Institute for Advanced Studies in Basic Sciences, Zanjan, 45195-1159, Iran
E-mail: miri@iasbs.ac.ir

Ramin Golestanian
Department of Physics and Astronomy, University of Sheffield, Sheffield S3 7RH, UK
E-mail: r.golestanian@sheffield.ac.uk

Abstract. As the technological advances lead to miniaturization of mechanical devices, engineers face new challenges that are brought about by the fundamentally different rules that apply at small scales. One of the biggest problems in small machines is the excessive wear of the many surfaces that work in contact with each other, which severely constrains the durability of such machine parts. Here, a force that is caused by the quantum fluctuations of electromagnetic field— known as the lateral Casimir force—is employed to propose a design for a potentially wear-proof rack and pinion with no contact, which can be miniaturized to nano-scale. We demonstrate that both uniform and harmonic lateral motion of the rack can be converted into unidirectional rotation of the pinion. The robustness of the design is studied by exploring the relation between the pinion velocity and the rack velocity in the different domains of the parameter space. The effects of friction and added external load are also examined.

1. Introduction

In recent years we have been witnessing a paradigm change in the technical problems involved in constructing miniaturized mechanical devices and the strategies to resolve them. In particular, tribological interactions, i.e. friction, adhesion, and wear, appear to pose new challenges at small length scales [1]. The abundance of surfaces in contact in small devices and high friction are problematic, and the traditional use of lubricants does not work because they become excessively viscous when made into molecular layers [2]. Devices with sliding surfaces in contact are known to wear out too rapidly [3], and it seems that strategies to minimize contact between the surfaces are needed to help make them more durable. The presence of short-ranged attractive dispersion or Casimir forces can cause tiny elements in small devices to stick together and bring the devices to stop [4], and a line of ongoing active research is focused on devising novel techniques to avoid such effects [5, 6]. In light of these technical difficulties, it seems desirable to have novel designs for mechanical devices that can operate without physical contact between their parts.

As a key interaction at nano-scale, Casimir force can be harnessed and used in small devices, as demonstrated by Capasso and collaborators who developed an actuator powered by the normal

© 2007 IOP Publishing Ltd

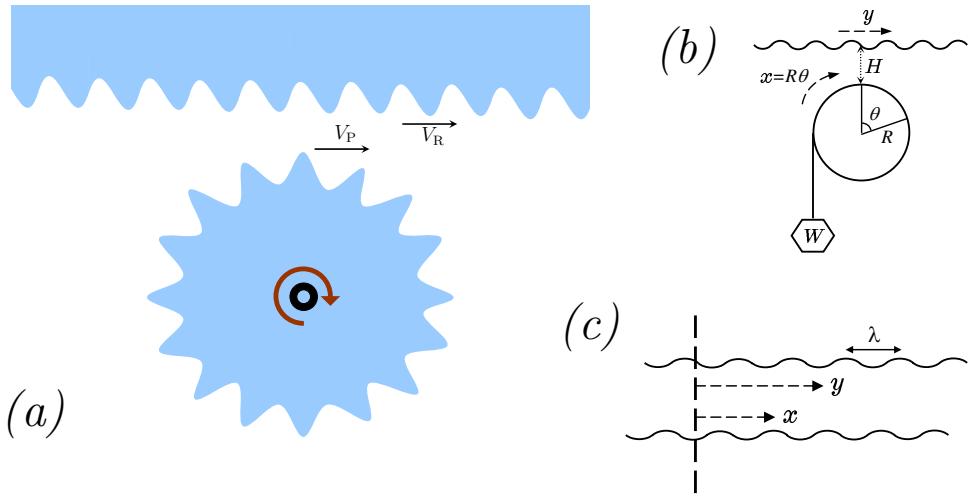

Figure 1. *(a)* The rack and pinion with no contact. *(b)* The schematics of the rack and pinion with an external load W. Corrugations of the cylinder are not shown. *(c)* Two corrugated plates with lateral shift $x - y$. The equilibrium position is at $x = y$.

Casimir force between a flat plate and a sphere [7, 8]. To avoid the limited applicability that the parallel-plate geometry might offer, it turns out that by making the two surfaces corrugated one can produce a lateral component to the Casimir force as has been recently proposed [9] and indeed verified experimentally [10]. The lateral Casimir force between corrugated surfaces, provides a possibility for friction-less transduction of lateral forces in nano-mechanical devices without any physical contact between them. The coupling between two surfaces via the quantum vacuum is realized by a term proportional to the sinus of the phase difference between them, reminiscent of the Josephson coupling between superconductors [9, 11], as it is a macroscopic manifestation of quantum coherence. Because the coupling is nonlinear, its mechanical response could involve oscillatory and unstable behavior similar to the what is observed in Ref. [8] for the case the device is powered by the normal Casimir force.

Here we make use of the lateral Casimir force to design a nano-scale rack and pinion without intermeshing, as shown in Fig. 1*(a)* [12, 13]. Our system consists of a corrugated plate (rack) and a corrugated cylinder (pinion) that are kept at a distance from each other. The pinion could be subject to external load (see Fig. 1*(b)*), and could experience friction when rotating around its axis. We demonstrate that both *uniform* [12] and *harmonic* [13] motion of the rack can be converted into unidirectional rotation of the pinion. For uniform motion of the rack with a velocity V_R, we find that the "contact" pinion velocity V_P (see Fig. 1*(a)*) is locked in to the rack velocity for sufficiently small values of V_R, and that there is a threshold rack velocity at which the pinion undergoes a *skipping transition* where the pinion can no longer hold the cogs in perfect registry with the rack. In the skipping regime, we find that the average pinion velocity can be both positive and negative (with $V_R > 0$) depending on the initial phase mismatch between the corrugations. The effects of the external load and friction are considered and the regions in the parameter space where the pinion can do work against the load are determined. These studies could help us examine the feasibility and efficiency of such a design as a mechanical transducer.

2. Lateral Casimir Force

When two sinusoidally modulated plates with identical wavelengths of λ are shifted with respect to each other by a length $x - y$ (see Fig. 1*(c)*), the lower plate experience the lateral Casimir

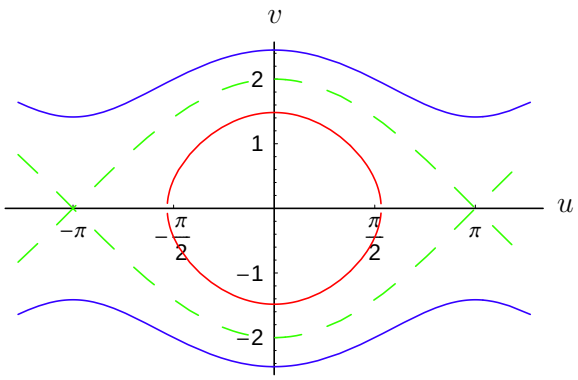

Figure 2. Phase portrait of the simple pendulum is periodic in u with a period of 2π. The dashed lines are the homoclinic orbits. Fixed points $(0,0)$ and $(\pm\pi,0)$ are the center and saddle points, respectively.

force [9, 11]

$$F_{\text{lateral}} = -F \sin\left[\frac{2\pi}{\lambda}(x-y)\right], \tag{1}$$

where the amplitude F depends on the mean separation of the plates and the amplitude of corrugations [10, 14, 15]. The amplitude of the lateral Casimir force for two parallel plates is

$$F_{\text{plate}} = \frac{2\pi\hbar c a_1 a_2 A}{\lambda H^5}\, J(H/\lambda), \tag{2}$$

where a_1 and a_2 are the two amplitudes of corrugation, H is the mean separation between the plates, and A is the surface area of the plates. The function $J(x)$ is a "Josephson" coupling that starts from the constant $\pi^2/120$ at small x and decays exponentially at large x [14]. Experimentally measured values of the lateral Casimir force (between a plate and a sphere of radius 100 μm) are in the 0.1 pN range for $\lambda = 1.1$ μm, $H \sim 200 - 300$ nm, $a_1 = 60$ nm, $a_2 = 8$ nm [10].

3. Theoretical Formulation

We can now use the lateral Casimir force in our design of the rack and pinion. The force introduces a net torque on the pinion, which plays the central role in the equation of motion for the coordinate $x = R\theta$ (Fig. 1*(b)*). The equation of motion reads

$$\frac{I}{R}\frac{d^2x}{dt^2} = -RF \sin\left[\frac{2\pi}{\lambda}(x-y)\right] - \frac{\zeta}{R}\frac{dx}{dt} - RW, \tag{3}$$

where I is the moment of inertia of the pinion about its major axis, ζ is the rotational friction coefficient, and W is an external load against which the pinion should do work.

We mainly focus on the uniform motion of the rack with a velocity V_{R}, i.e. $y = V_{\text{R}}t$, expect for a final section where we consider the case of a vibrating rack. The nonlinear equation 3 can be better studied in the phase plane $(u \equiv 2\pi(x-y)/\lambda, v = \dot{u})$, where it reads $\dot{u} = v$, $\dot{v} = -\sin u - \epsilon(v - v_0) - W/F$. In the above equations, we have measured the time in units of $T = \sqrt{I\lambda/(2\pi F R^2)}$, and have defined the dimensionless parameter $\epsilon = T\zeta/I$, which is a measure of the relative importance of friction in the system. The parameter $v_0 = \dot{u}_0 = 2\pi(\dot{x}_0 - V_{\text{R}}T)/\lambda$ is the initial value for v. A key velocity scale is given by

$$V_{\text{S}} = \frac{\lambda}{2\pi T} = \left(\frac{F\lambda R^2}{2\pi I}\right)^{1/2}, \tag{4}$$

which corresponds to the velocity at which the kinetic energy of the rotating pinion is of the order of the work done by the lateral Casimir force upon displacement by one tooth. As we will

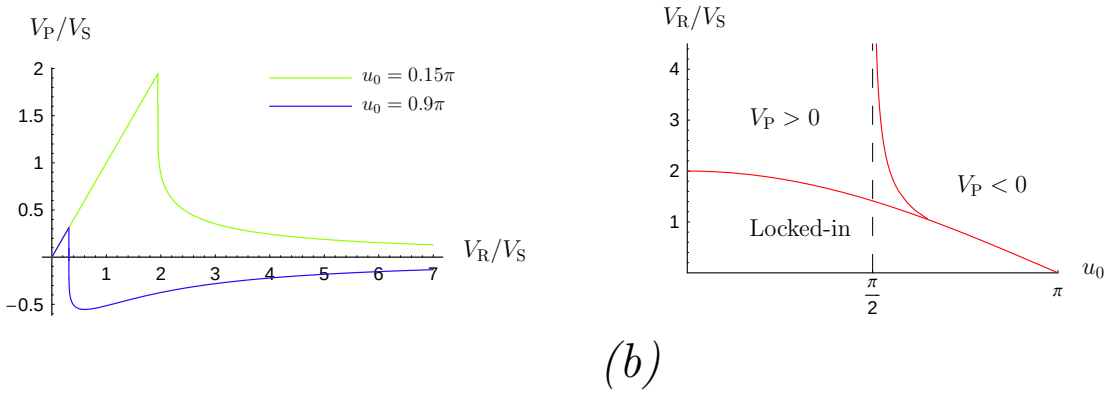

(a) *(b)*

Figure 3. *(a)* Pinion velocity versus rack velocity in the absence of dissipation and external load. The behavior of the system after skipping transition depends crucially on the initial phase mismatch u_0. *(b)* Domains of positive and negative pinion velocities as well as the phase boundary for the skipping transition. Only half of the plot is shown due to $u_0 \to -u_0$ symmetry in this case.

see below, the quantity $F\lambda$ can be considered as the effective "bond strength" of the coupling between the pinion and rack, so that a "bound state" between them can only tolerate pinion kinetic energies of this order or magnitude, which means that Eq. 4 gives the *skipping velocity*. For simplicity, we only consider the case of pinions that are initially at rest throughout this paper ($\dot{x}_0 = 0$), which means $v_0 = -V_R/V_S$, although the formulation can be readily used to study other initial conditions as well.

The nonlinear force coupling in the dynamical equation as well as the effects of friction and external load will determine the performance of the system and can create a variety of different regimes. These issues are addressed in the following section.

4. Results and Discussion

4.1. No dissipation

In the absence of dissipation and load, Eq. 3 is identical to the celebrated nonlinear plane pendulum problem [16]. It is well known that for this system, the *energy*

$$h = \frac{1}{2}v^2 + 1 - \cos u = \frac{1}{2}\left(\frac{V_R}{V_S}\right)^2 + 1 - \cos u_0, \tag{5}$$

is a constant of motion, and there are two families of periodic orbits, corresponding to rotations ($h > 2$) and oscillations ($h < 2$). The system has the phase portrait of Fig. 2, with a pair of homoclinic orbits $(u_0^{\pm}, v_0^{\pm}) = (\pm 2\tan^{-1}(\sinh t), \pm 1/\cosh t)$ of energy 2 [16]. For $0 < h < 2$, the system is oscillatory with a period of $4K(\sqrt{h/2})$, where $K(m) = \int_0^{\pi/2} d\theta (1 - m^2 \sin^2\theta)^{-1/2}$ is the complete elliptic integral of the first kind [17]. In this case $|u| \leq |\cos^{-1}(1-h)| \leq \pi$, which means that the distance $|x - y|$ between the teeth of the rack and pinion does not exceed $\lambda/2$. Thus the pinion is locked-in with the rack and will have a forward motion with superimposed oscillations (jerks). In the case of $h > 2$, the system is not locked in any more and depending on the initial conditions it can have different behaviors.

The value of h, which determines the behavior of the system, depends on V_R and u_0 (see Eq. 5). For $V_R < V_S\sqrt{2(1+\cos u_0)}$ the rack and pinion are geared up and we have $V_P = V_R$ for the jerk–averaged pinion velocity. Higher rack velocities $V_R > V_S\sqrt{2(1+\cos u_0)}$ cause the system to go to the "rotation" phase of the equivalent pendulum problem, which means that

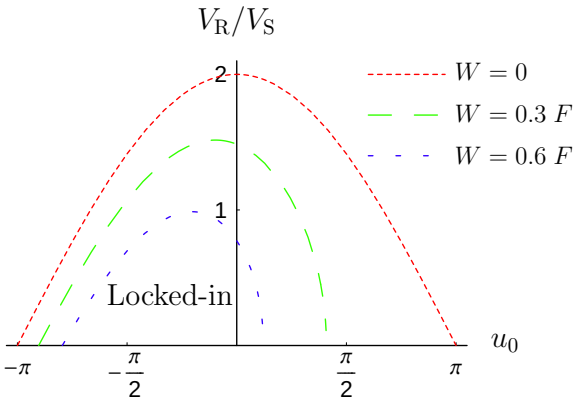

Figure 4. Phase boundary for the skipping transition, in the absence of dissipation, as a function of the external load.

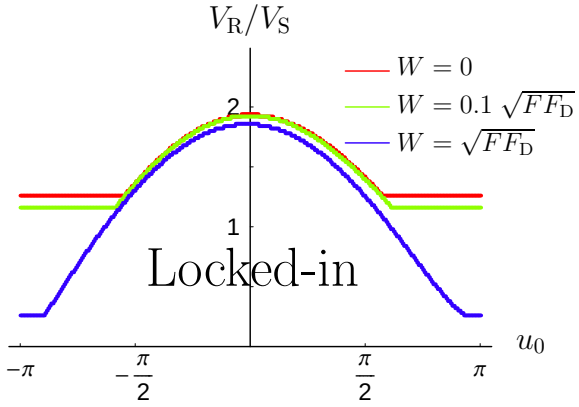

Figure 5. Phase boundary for the skipping transition, in the presence of weak dissipation, as a function of the external load for $\sqrt{F_D/F} = 0.05$.

the pinion skips teeth with respect to the rack, but will still have a net average velocity. This *pinion velocity*, which is defined as the time-average velocity over one full period of oscillation, can be calculated as

$$V_P = V_R - \frac{\pi V_S}{\sqrt{2/h}\,K\left(\sqrt{2/h}\right)}, \tag{6}$$

where h is given by Eq. 5. In Fig. 3*(a)*, the pinion velocity is plotted as a function of the rack velocity for two values of the initial phase mismatch ($u_0 = 0.15\pi$ and $u_0 = 0.9\pi$). The pinion velocity rises linearly with the rack velocity initially and then drops abruptly at the skipping transition. At large rack velocities $V_R \gg V_S$, the pinion velocity has an asymptotic form $V_P = \cos u_0 V_S^2/V_R + \cdots$, which shows that it vanishes at infinity, and that the decay can be both from below (for $u_0 > \pi/2$) and above (for $u_0 < \pi/2$). An intriguing feature in the solution is possibility of dropping into negative pinion velocities—the *reverse gear*—after the skipping transition, as Fig. 3*(a)* shows. Figure 3*(b)* delineates the different domains of phase lock-in, forward motion, and reverse motion, in the space of the rack velocity and the phase mismatch. One can see that for $0 < u_0 < \pi/2$ the average velocity is always positive, while for $\pi/2 < u_0 < \pi$ the pinion velocity can be switched from positive to negative by increasing V_R/V_S. This can be achieved by either speeding up the rack or decreasing the skipping velocity by increasing the separation between the rack and pinion (see below).

4.2. The effect of external load

In the absence of dissipation, Eq. 3 has $h' = v^2/2 + 1 - \cos u + Wu/F$ as the constant of motion. The center and saddle fixed points are located at $(-\sin^{-1}(W/F), 0)$ and $(-\pi + \sin^{-1}(W/F), 0)$, respectively. Two classes of motion are separated by the homoclinic orbit (or the saddle-loop) of energy $h'_s = 1 + \sqrt{1-(W/F)^2} - [\pi - \sin^{-1}(W/F)](W/F)$, leading to rotations for $h' > h'_s$ and oscillations for $h' < h'_s$, in the equivalent pendulum problem. Figure 4 shows the domains for two different regimes as well as the boundary for the skipping transition as a function of the rack velocity and the initial phase mismatch. As the load is increased, the two fixed point approach each other thereby narrowing down the locked-in region, until at $W = F$ it disappears when they fully merge. Therefore, $W < F$ is a necessary condition to have positive rack velocities. Note that the entire skipping region corresponds to $V_P < 0$ because the constant of motion prohibits unlimited buildup of positive values of u for any non-vanishing W/F.

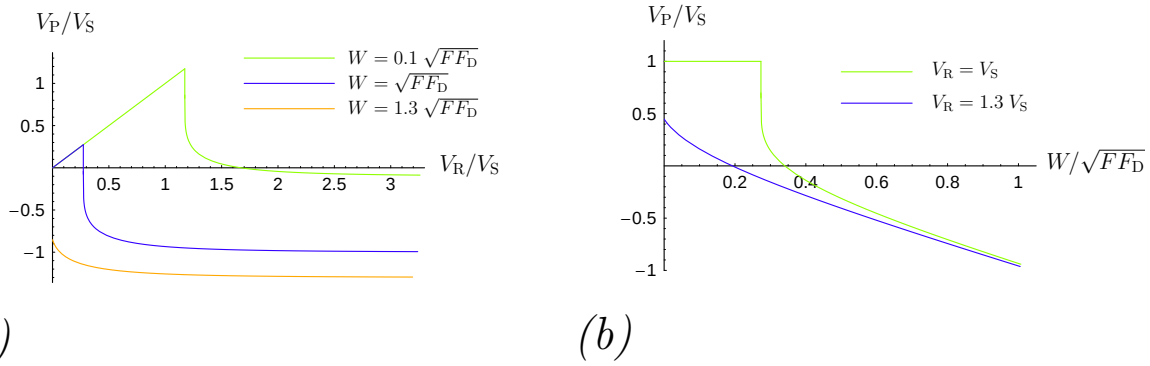

(a) *(b)*

Figure 6. *(a)* Pinion velocity versus rack velocity in the presence of weak dissipation and external load. The behavior of the system after skipping transition depends crucially on the load. *(b)* Force–velocity response of the rack and pinion could be of two general forms depending on the value of the rack velocity. Both figures correspond to values of u_0 for which the skipping transition threshold is independent of the phase mismatch, namely the horizontal parts of the boundaries in Fig. 5.

4.3. Weak dissipation

The dynamical system described by Eq. 3 is not integrable in the presence of the dissipation term, as energy is not conserved anymore. If the dissipation is weak, such that $\zeta V_R/R^2 + W < F$, we can use the Melnikov method [16, 18] to study the perturbed phase portrait of the system (see Appendix for details). In this regime, the force scale

$$F_D = \frac{\zeta^2 \lambda}{2\pi I R^2}, \tag{7}$$

seems to play an important role. (Note that $\zeta V_S/R^2 = \sqrt{FF_D}$.)

Similar to when there is no dissipation, the system develops the two class of commensurate and incommensurate motion transduction separated by a skipping transition boundary. Figure 5 shows an example of this phase diagram that has been calculated numerically, for different values of the external load. The phase boundary is found to consist of horizontal (u_0-independent) parts that are met by a bell-shaped central part reminiscent of that of the dissipation-less system. In the part that does not depend on u_0, we find that for $\zeta V_R/R^2 < \frac{4}{\pi}\sqrt{FF_D} - W$ the system is in the locked-in phase and we have $V_P = V_R$. As the rack velocity is increased above this limit, the system undergoes a skipping transition. The pinion velocity for $\zeta V_R/R^2 > \frac{4}{\pi}\sqrt{FF_D} - W$ can be found from Eq. 6, with a value $h = h_m$ that is a solution to this equation

$$V_R + WR^2/\zeta = \frac{4}{\pi} V_S \sqrt{h_m/2}\, E\left(\sqrt{2/h_m}\right), \tag{8}$$

where $E(m) = \int_0^{\pi/2} d\theta \sqrt{1 - m^2 \sin^2\theta}$ is the complete elliptic integral of the second kind [17]. Figure 6*(a)* shows the pinion velocity as a function of the rack velocity for different values of the external load. The general feature of drastic drop in the pinion velocity after the skipping transition is observed, and the asymptotic behavior of the pinion velocity at large rack velocities is $V_P = -WR^2/\zeta + \frac{1}{2}V_S^4/V_R^3 + \cdots$, which shows a complete decoupling in the system (signalled in the saturation velocity of $-WR^2/\zeta$) at infinitely large rack velocities. The response of the system in the bell-shaped region of the phase diagram of Fig. 5 will lead to similar results and can be obtained numerically. Note that the Melnikov approximation breaks down for large rack

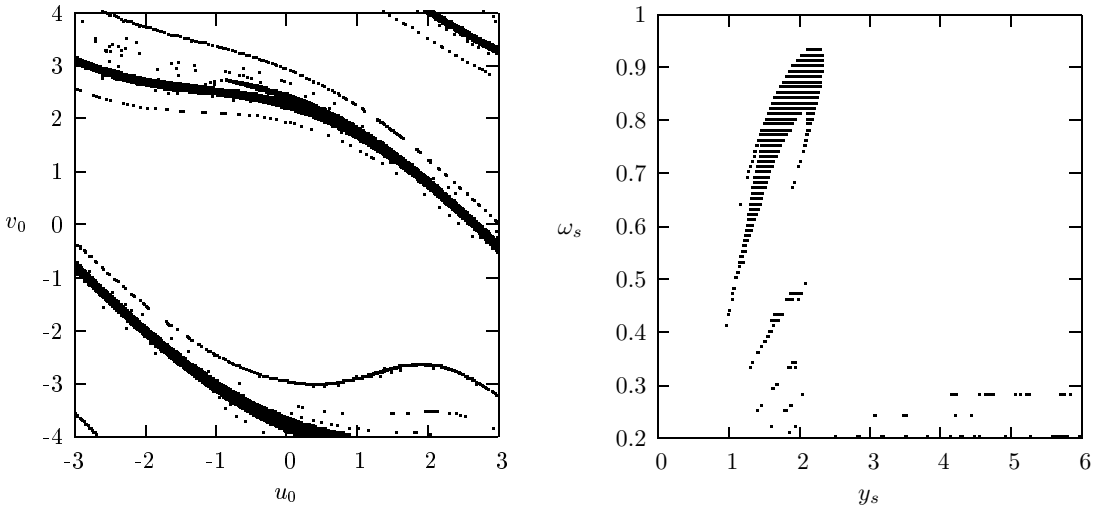

Figure 7. *(a)* Basins of attraction for $y_s = 1.4$, $\omega_s = 2/3$, $\phi_s = 0$, $\epsilon = 0.5$, $m = n = 1$, and $W = 0.185\ F$. These initial conditions lead to $V_{\rm P} > 0$. *(b)* Values of y_s and ω_s which lead to $m = n = 1$. Here $x_0 = 0$, $\dot{x}_0 = 0$, $\epsilon = 0.5$, and $W = 0.1\ F$.

velocities and we need a complementary approach to examine the behavior of the system in that limit (see below).

The force–velocity response of the system in the u_0-independent region can also be extracted from this result. Figure 6*(b)* shows the pinion velocity as a function the external load for two values of the rack velocity ($V_{\rm R} = V_{\rm S}$ and $V_{\rm R} = 1.3\ V_{\rm S}$). For $V_{\rm R} < \frac{4}{\pi}V_{\rm S}$, the pinion velocity is independent of the load for $W < \frac{4}{\pi}\sqrt{FF_{\rm D}} - \zeta V_{\rm R}/R^2$, and drops drastically after the onset of skipping, whereas the decrease upon introduction of load starts from the beginning when $V_{\rm R} > \frac{4}{\pi}V_{\rm S}$. One can identify the load at which the pinion velocity vanishes as the *stall force*.

4.4. Strong dissipation

The Melnikov method fails if $\zeta V_{\rm R}/R^2 + W \geq F$, in which limit we can proceed by neglecting the acceleration term $\dot{v} = \ddot{u}$ in Eq. 3. This allows us to solve the equation in closed form, yielding $u(t) = 2\tan^{-1}\left[\left(\frac{F}{\zeta V_{\rm R}/R^2+W}\right) - \sqrt{1-\left(\frac{F}{\zeta V_{\rm R}/R^2+W}\right)^2}\ \tan\left(\frac{\pi t}{\tau}\right)\right]$, where $\tau = \lambda/\sqrt{(V_{\rm R} + WR^2/\zeta)^2 - (FR^2/\zeta)^2}$. The explicit expression for u can be to calculate the time-averaged pinion velocity

$$V_{\rm P} = V_{\rm R} - \sqrt{(V_{\rm R} + WR^2/\zeta)^2 - (FR^2/\zeta)^2}, \tag{9}$$

which produces very similar curves to those plotted in Fig. 6*(a)* above the skipping transition using the Melnikov method. The stall force (load) in this limit can be found as $W_s = F\left[\sqrt{1+(\zeta V_{\rm R}/FR^2)^2} - (\zeta V_{\rm R}/FR^2)\right]$. Interestingly, Eq. 9 gives a limiting value of $V_{\rm P} = -WR^2/\zeta$ at large values of rack velocity, in agreement with the asymptotic behavior suggested by the Melnikov approach.

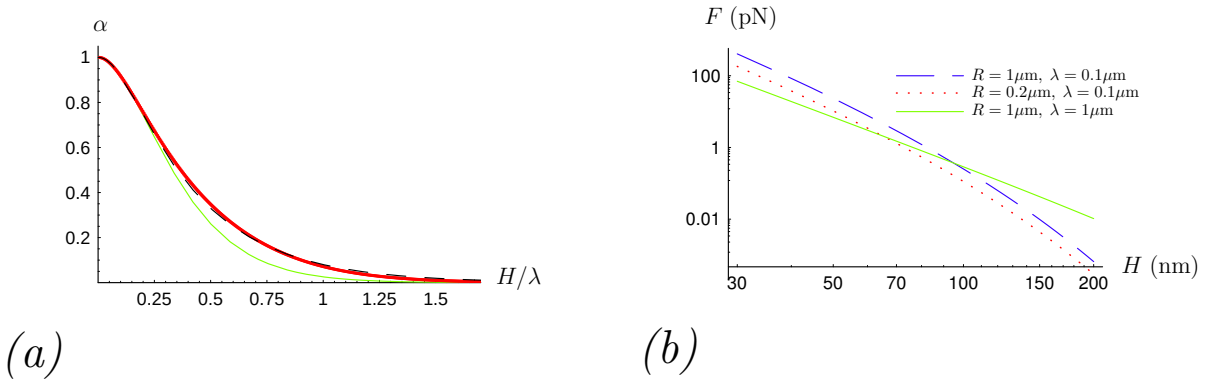

Figure 8. *(a)* The parameter α introduced in the text as a function of H/λ for perfect metals (red dots) compared to the pairwise summation approximation (green solid line). The dashed-line shows the empirical formula presented in the text. *(b)* Amplitude of the lateral Casimir force as a function of the gap size for perfect metallic boundaries, corresponding to $a_1 = a_2 = 10$ nm and $L = 10\mu$m, for different values of radius and corrugation wavelength. Note that for the case of $R = 0.2\mu$m (dotted curve), the larger separations in the plot are approaching the limit of validity of the PFA approximation.

4.5. Vibrating Rack

Now we consider harmonic motion of the plate, i.e. $y = y_p \cos(\omega_p t + \phi_p)$. As before, we introduce $u = 2\pi(x-y)/\lambda$ and measure the time in units of $T = \sqrt{I\lambda/(2\pi FR^2)}$ to rewrite the nonlinear equation 3 as $\ddot{u} = -\sin u - \epsilon\dot{u} - \frac{W}{F} + y_s \cos(\omega_s t + \phi_s)$, where $\epsilon = T\zeta/I$, $\omega_s = \omega_p T$, $y_s = y_p\omega_p I\left[\omega_p^2 + \zeta^2/I^2\right]^{1/2}/(FR^2)$, and $\phi_s = \phi_p - \tan^{-1}[\zeta/(I\omega_p)]$. Following Refs. [19, 20], we expect *pairs* of period steady-state solutions $(u^*, v^* = \dot{u}^*)$ such that $u^*(t+2\pi n/\omega_s) = u^*(t) \pm 2\pi m$ and $v^*(t + 2\pi n/\omega_s) = v^*(t)$. Here m and n are integer numbers. In the following, we focus on the upward motion of the load or positive average velocities. The average pinion velocity in this case is deduced from $\overline{v^*} = m\omega_s/n$, namely

$$V_{\rm P} = \frac{m}{n}\left(\frac{\lambda\omega_p}{2\pi}\right). \tag{10}$$

Averaging the equation of motion in the time interval $2\pi n/\omega_s$ yields $-W/F - \epsilon\overline{v^*} = \overline{\sin u^*}$ which necessitates $W < F(1 - \epsilon\omega_s m/n)$. With the anzats $u^* \approx u_0 + \overline{v^*}t + \Delta n/\omega_s \sin(\omega_s t/n)$ and the identity $\exp(iz\cos\beta) = \sum_{k=-\infty}^{\infty} i^k J_k(z)\exp(ik\beta)$ in terms of the Bessel function $J_k(z)$, a stronger criterion of $W < F\left[|J_n(n\Delta/\omega_s)| - \epsilon\omega_s m/n\right]$ can be obtained. Note that the initial conditions u_0 and v_0 must be tuned to ensure $V_{\rm P} > 0$. In Fig. 7*(a)*, we have shown the basins of attraction for $y_s = 1.4$, $\omega_s = 2/3$, $\phi_s = 0$, $\epsilon = 0.5$, $m = n = 1$, and $W = 0.185\ F$. The steps of u_0 and v_0 are 0.02. Our numerical calculations show that upward motion of the load ceases at $W = 0.192\ F$, consistent with our analytical estimate of $W < 0.249\ F$ obtained via $J_1(\Delta/\omega_s) < 0.582$.

It is interesting that the driving parameters can be tuned to set the integers m and n which determine the average pinion velocity. Figure 7*(b)* shows the parameters y_s and ω_s which lead to $m = n = 1$. In these calculations the steps of y_s and ω_s are taken to be 0.01, and the chaotic states were avoided by checking the negativeness of the largest Lyapunov exponent of the system [21].

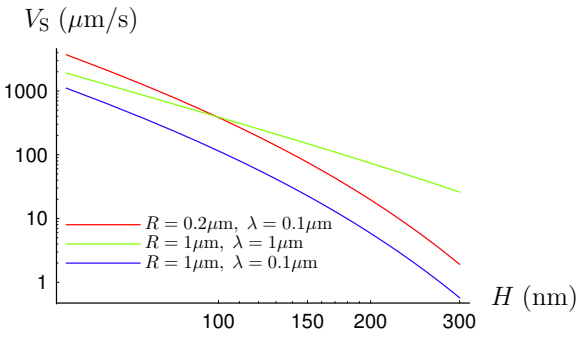

Figure 9. Skipping velocity as a function of the gap size for perfect metallic boundaries, corresponding to $\rho = 19.3$ gr/cm^3 (gold) and $a_1 = a_2 = 10$ nm, for different values of radius and corrugation wavelength.

5. Concluding Remarks

We have presented above a range of interesting behaviors for the proposed rack and pinion, and in order to make a stronger link to the experiments we need to quantify the amplitude of the lateral Casimir force F. For a cylinder of radius R located at a (nearest) distance H from a plate (see Fig. 1*(b)*), the Casimir interaction can be calculated from the corresponding interaction between two parallel plates, using the Proximity Force Approximation (PFA)[22]. For the normal Casimir force between perfect metals, it has been recently shown that this approximation works surprisingly well for $H \leq R$ [23]. Using PFA for the lateral Casimir force between a pinion of length L and corrugation amplitude a_1 and a rack of corrugation amplitude a_2 with $a_1, a_2 \ll H$, we find

$$F = \left(\frac{7\pi^4\sqrt{2}}{3072}\right) \frac{\hbar c a_1 a_2 L R^{1/2}}{\lambda H^{9/2}}\, \alpha\left(\frac{H}{\lambda}\right), \tag{11}$$

to the leading order, where $\alpha = \frac{3072}{7\pi^3}\int_1^\infty \frac{dt}{t^5\sqrt{t-1}} J\left(\frac{H}{\lambda}t\right)$ with J being the ("Josephson–") coupling function presented in Ref. [14]. Figure 8*(a)* shows the dependence of α on H/λ for perfect metals and a comparison to pairwise summation approximation, with the dashed-line showing an empirical approximate formula $\alpha_e = 1/\cosh^{4/9}\left(\frac{12\pi}{\sqrt{35}}\frac{H}{\lambda}\right)$ which could be useful for practical purposes. Figure 8*(b)* shows the amplitude of the lateral Casimir force as a function of the separation for a typical system.

Using the above result for the amplitude, we can calculate the skipping velocity as

$$V_S = \left(\frac{7\pi^2\sqrt{2}}{3072}\right)^{1/2} \left(\frac{\hbar c}{\rho H^4}\right)^{1/2} \left(\frac{a_1 a_2}{H^2}\right)^{1/2} \left(\frac{H}{R}\right)^{3/4} \alpha^{1/2}, \tag{12}$$

where ρ is the mass density of the pinion. This result shows a strong power law behavior at small values of H followed by an exponential decay at large H whose length scale is set by λ. Figure 9 shows the skipping velocity as a function of the gap size, for different values of the radius and wavelength. The typical values for V_S, which correspond to velocities that the system transfer robustly, are remarkably high: translated into angular velocity it is in the kHz region. The strong dependence of the skipping velocity on the gap size can be used to move in the parameter space and change the behavior of the system. For example, by increasing H and reducing V_S one can move in the vertical direction in the phase diagram of Fig. 3*(b)* and switch from the locked-in phase to a reverse gear, at constant rack velocity. In other words, changing the separation provides a continuous analogue of clutch–gear system. The calculations presented here have been based on the assumption of perfect metallic boundaries, and one expects corrections for gap sizes smaller than the plasma wavelength of the metals [15].

The value of the friction coefficient ζ is also instrumental in determining the behavior of the system. While this quantity is highly system-dependent in general, it is interesting to note

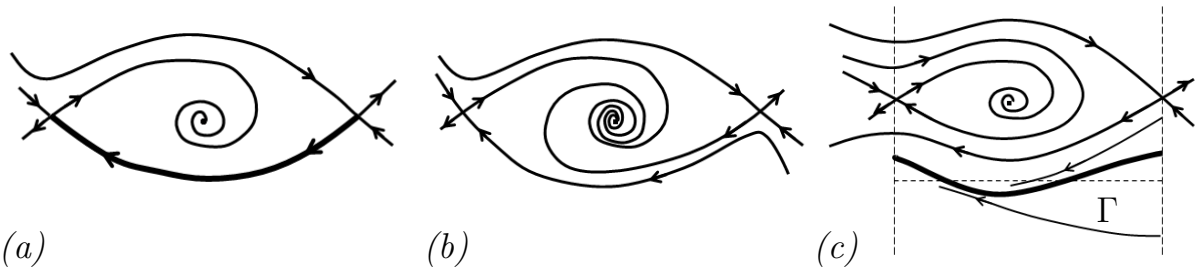

Figure A1. Phase portrait for the rack and pinion. *(a)* $v_0 = v_\epsilon - 4/\pi$; *(b)* $v_0 > v_\epsilon - 4/\pi$; *(c)* $v_0 < v_\epsilon - 4/\pi$. Γ is a unique attracting closed orbit.

that a contribution to dissipation also comes from the interplay between the electromagnetic fluctuations and the dielectric loss properties of the two objects [24].

In conclusion, we have proposed a design for a nano-scale rack and pinion without contact by employing the quantum fluctuations of the electromagnetic field. This design, and the corresponding variants that could be readily conceived, might help towards making more durable machine parts for small mechanical system.

Acknowledgments
This work was supported by EPSRC under Grant EP/E024076/1.

Appendix A. Melnikov Method

Weak dissipation which perturbs the integrable plane pendulum system can be dealt with using the Melnikov method [18] which is exposed in [16, 21, 19]. We assume $\epsilon|v_0 - v_\epsilon| < 1$, where $v_\epsilon = W/(F\epsilon) = W/\sqrt{FF_{\rm D}}$. As Fig. A1 sketches, the phase portrait for the rack and pinion depends on the sign of $v_0 - v_\epsilon + 4/\pi$. Supposing an initial condition $\dot{x}_0 = 0$ or $v_0 < 0$, the exceptional case $v_0 = v_\epsilon - 4/\pi$ may happen if $v_\epsilon < 4/\pi$. Here the lower homoclinic orbit survives, and the fixed point $P_1 = \left(\sin^{-1}(\epsilon v_0 - \epsilon v_\epsilon), 0\right)$ is an attractor [Fig. A1*(a)*]. In the case of $v_0 > v_\epsilon - 4/\pi$ where $v_\epsilon < 4/\pi$, the domain of attraction of P_1 is the entire phase plane [Fig. A1*(b)*], which leads to a stationary value of $v = 0$, i.e. the velocities of pinion and rack are the same. The case of $v_0 < v_\epsilon - 4/\pi$ is more intricate. Bendixson's criterion can be invoked to show that none of the closed orbits encircling the center in Fig. 2 is preserved under the perturbation [16], and the point P_1 is an attractor for them. Furthermore, it can be shown that a closed orbit Γ lying below the homoclinic orbits and encircling the phase cylinder persists, and is an attractor [Fig. A1*(c)*]. Now it can be anticipated that initial conditions in the domain of attraction of P_1 ultimately yield $v = 0$. For initial conditions in the domain of attraction of Γ, the average velocity is given by Eq. 6 where $h = h_m$ is used as a solution of Eq. 8.

References

[1] Carpick RW 2006 *Science* **313** 184
[2] Hu YZ and Granick S 1998 *Trib. Lett.* **5** 81
[3] de Boer MP and Mayer TM 2001 *MRS Bull.* **26** 302
[4] Buks E and Roukes ML 2001 *Phys. Rev.* B **63** 033402
[5] Socoliuc A, Gnecco E, Maier S, Pfeiffer O, Baratoff A, Bennewitz R and Meyer E 2006 *Science* **313** 207
[6] Park JY, Ogletree DF, Thiel PA, and Salmeron M 2006 *Science* **313** 186
[7] Chan HB, Aksyuk VA, Kleiman RN, Bishop DJ and Capasso F 2001 *Science* **291** 1941
[8] Chan HB, Aksyuk VA, Kleiman RN, Bishop DJ and Capasso F 2001 *Phys. Rev. Lett.* **87** 211801
[9] Golestanian R and Kardar M 1997 *Phys. Rev. Lett.* **78** 3421
[10] Chen F, Mohideen U, Klimchitskaya GL and Mostepanenko VM 2002 *Phys. Rev. Lett.* **88** 101801
[11] Golestanian R and Kardar M 1998 *Phys. Rev. A* **58** 1713

[12] Ashourvan A, Miri MF and Golestanian R 2007 *Phys. Rev. Lett.* **98** 140801
[13] Ashourvan A, Miri MF and Golestanian R 2007 *Phys. Rev.* E **75** 040103 (R)
[14] Emig T, Hanke A, Golestanian R and Kardar M 2003 *Phys. Rev. A* **67** 022114
[15] Rodrigues RB, Maia Neto PA, Lambrecht A and Reynaud S 2006 *Phys. Rev. Lett.* **96** 100402
[16] Guckenheimer J and Holmes P 1983 *Nonlinear Oscillations, Dynamical Systems, and Bifurcations of Vector Fields* (Berlin: Springer)
[17] Gradshteyn IS and Ryzhik IM 2000 *Table of Integrals, Series, and Products* 6th edition (New York: Academic Press)
[18] Melnikov VK 1963 *Trans. Moscow Math. Soc.* **12** 1
[19] Belykh VN, Pedersen NF and Sorensen OH 1977 *Phys. Rev.* B **16** 4853
[20] Gwinn EG and Westervelt RM 1986 *Phys. Rev.* A **33** 4143
[21] Argyris JH, Faust G and Haase M 1994 *An Exploration of Chaos* (Amsterdam: North-Holland)
[22] Derjaguin B 1934 *Kolloid-Z.* **69** 155
[23] Emig T, Jaffe RL, Kardar M and Scardicchio A 2006 *Phys. Rev. Lett.* **96** 080403
[24] Pendry JB 1997 *J. Phys.: Condens. Matter* **9** 10301